Liver-secreted fluorescent blood plasma markers enable chronic imaging of microcirculation

Xiaowen Wang[1+], Christine Delle[1+], Antonis Asiminas[1+], Sonam Akther[1], Marta Vittani[1], Peter Brøgger[1], Peter Kusk[1], Camilla Trang Vo[1], Ayumu Konno[2,3], Hirokazu Hirai[2,3], Masahiro Fukuda[4,5], Pia Weikop[1], Steven A Goldman[1,6], Maiken Nedergaard[1,6*], Hajime Hirase[1,6*]

1. Center for Translational Neuromedicine, Faculty of Health and Medical Sciences, University of Copenhagen, Copenhagen, Denmark
2. Viral Vector Core, Gunma University Initiative for Advanced Research, Maebashi, Gunma 371-8511, Japan
3. Department of Neurophysiology & Neural Repair, Gunma University Graduate School of Medicine, Maebashi, Gunma 371-8511, Japan
4. Program in Neuroscience and Behavioral Disorders, Duke-NUS Medical School, Singapore, 169857 Singapore
5. International Research Center for Medical Sciences (IRCMS), Kumamoto University, Kumamoto, Japan
6. Center for Translational Neuromedicine, University of Rochester Medical Center, Rochester, NY, USA

+ contributed equally

* Correspondence should be addressed to Maiken Nedergaard (maiken_nedergaard@urmc.rochester.edu) or Hajime Hirase (hirase@sund.ku.dk)

Author contribution:

Designed research: XW, CD, AA, SA, MF, SG, MN, HaH; Performed research: XW, CD, SA, CVT, MV, PB, PK, AK; Contributed unpublished reagents/analytic tools: AK, HiH; Analyzed/interpreted data: XW, CD, AA, SA, CVT; Wrote the paper: AA, CD, XW, MF, MN, HaH

Acknowledgments: We thank Dr. Jean-Charles Paterna (University of Zurich Viral Vector Facility) for technical support on AAV vectors. We also thank members of the Center for Translational Neuromedicine for comments on earlier versions of the manuscript. The authors declare no competing financial interests.

Sources of Funding: This work was supported by the Novo Nordisk Foundation (HaH, NNF19OC0058058), Danmarks Frie Forskningsfond (0134-00107B), the Olav Thon Foundation (MN), the Lundbeck Foundation (MN), the program for Brain Mapping by Integrated Neurotechnologies for Disease Studies (HiH, Brain/MINDS, JP20dm0207057 and JP21dm0207111) by the Japan Agency for Medical Research and development (AMED) and JSPS KAKENHI (AK,) by MEXT, Japan.

Key words:

Recombinant protein, *in vivo* imaging, microcirculation, chronic, vasculature, hyperemia, cerebral blood flow

Abstract

Studying blood microcirculation is vital for gaining insights into vascular diseases. Acute administration of fluorescent tracers is currently used for deep tissue blood flow imaging. This is invasive, and the plasma fluorescence decreases within an hour of administration. We report a novel approach for the longitudinal study of vasculature. Using a single systemic administration of viral vectors, we express fluorescent secretory albumin-fusion proteins in the liver to label the blood in mice. All segments of the vasculature in brain and peripheral tissue are observable by two-photon microscopy within two weeks of vector administration. This approach allows for observation of circulation without the need for repeated administration for several months. We demonstrate the chronic assessment of vascular functions at micro- and mesoscopic scales. This genetic plasma labeling approach represents a versatile and cost-effective method for the chronic investigation of vasculature functions across the body in health and disease.

Introduction

The vascular system is an impressive network of vessels providing rapid supply of nutrients and oxygen to tissues and organs throughout the body. The human vascular system reaches a length of nearly 100,000 km, through which the blood circulates within the dense network of capillaries in a matter of a minute (50-80 s).[1] In humans, capillaries have a diameter of 8–10 µm and form the capillary bed in tissues with a density of ~600/mm^3, where blood oxygen and metabolites are exchanged.[2] Advances in imaging technologies have provided many methods to visualize and study various aspects of circulation and metabolism. While magnetic resonance imaging (MRI) and positron emission tomography (PET) can capture images of entire body parts, optical imaging provides sufficient temporal and spatial resolutions to characterize the dynamics in individual vessels. In particular, two-photon microscopy provides high lateral spatial resolution (~1 µm) and deep parenchymal penetration (~1 mm). Hence, two-photon imaging has in recent years provided a wealth of information regarding the dynamic control of the microcirculation.[3–5]

Capillary blood flow is commonly visualized by introducing a fluorescent tracer into the blood plasma, whereby non-fluorescent blood cells appear dark.[5–7] Fluorescent molecules conjugated to large-fragment dextran [e.g., Fluorescein isothiocyanate-dextran (FITC-dextran), 2 MDa] are popular owing to the absence of immunological response and relatively long plasma lifetime of dextran.[8,9] However, this labeling approach has some important limitations. Introduction of dextran into the blood stream increases its viscosity and consequently reduces flow.[10–12] This may have significant implications for the physiological relevance of observations made with dextran blood plasma labelling. Also, the signal intensity of tracer-injected plasma attenuates significantly within an hour of administration, requiring additional intravenous injections for longer experiments. Crucially, awake *in vivo* studies require continuous or repeated tracer administration which introduces unwanted stress and increases the risk of developing an immune response. A minimally invasive method that allows for stable, long-term monitoring of vascular function will greatly accelerate studies of the microcirculation,

Human and rodent plasma albumin represents ~55% of total plasma protein at concentrations ~0.6 mM.[13] [14] The vast majority of plasma albumin (>90%) is synthesized in the liver and rapidly secreted into the bloodstream.[15] Therefore, albumin presents a prime candidate for the design of genetically encoded plasma tracers suitable for chronic imaging. Here we expressed a secretory recombinant fluorescent protein albumin-mNeonGreen[16] (Alb-mNG) in hepatocytes by intraperitoneal (i.p.) injection of adeno-associated viral vectors (AAVs) in mice. This genetically encoded racer was incorporated into the blood plasma, and cerebral capillary flow was reliably observable two weeks after virus injection without apparent signs of inflammation. Longitudinal imaging of cerebral capillaries allowed the evaluation of sensory-evoked hyperemia and blood-brain-barrier (BBB) permeability in response to lipopolysaccharide-induced inflammation. Overall, we demonstrate that the visualization of blood flow by liver-secreted albumin-conjugated fluorescent proteins represents a powerful approach to examine acute and chronic changes of vascular structure and function.

Results

Alb-mNG is a secretory protein

We first sought to determine the secretory nature of Alb-mNG. In hepatocytes, secretory mature albumin is derived from pre-proalbumin, which in turn is processed in the endoplasmic reticulum and Golgi apparatus to have N-terminus cleavages.[17] Therefore, we hypothesized that fusion of mNG to the C-terminus of albumin (Alb-mNG) will lead to the secretion of Alb-mNG extracellularly while N-terminus fusion (mNG-Alb) should mask the secretory signal and results in cytosolic accumulation. Accordingly, we transfected HEK293 cells with mammalian expression plasmids containing the Alb-mNG and mNG-Alb

constructs (Fig.1a-b). A secretory form of mNG containing the IgK leader signal peptide at the N-terminus (IgKL-mNG) was used as a positive control. HEK293T cells were imaged one and two days after transfection. Green fluorescence was observed in transfected cells with each of the three plasmids, and no apparent signs of abnormal morphology were observed.

As expected, IgKL-mNG and Alb-mNG expression resulted in dim cytosolic fluorescent signals and obvious culture medium fluorescence (two-way ANOVA: construct x time interaction, $p<0.05$; *post hoc* tests: IgKL-mNG vs mNG-Alb and Alb-mNG vs mNG-Alb, $p<0.05$ at both 24h and 48h time points; n=18; Fig 1c-e). Non-uniform intracellular localization was evident, possibly indicating intracellular trafficking or lysosomal processing. On the other hand, bright cytosolic expression was observed for mNG-Alb (Fig 1c). Secretion of IgKL-mNG and Alb-mNG was further confirmed by measurement of culture medium fluorescence using a plate reader 24 h and 48 h post-transfection (two-way ANOVA: construct x time interaction, $p<0.05$; *post hoc* tests: IgKL-mNG vs mNG-Alb and Alb-mNG vs mNG-Alb, $p<0.05$ at both 24h and 48h time points; n=6; Fig 1e). Notably, medium fluorescence increased over time, suggesting stability and accumulation of the secreted proteins. These observations indicated that C-terminus fusion of albumin to fluorescent proteins can function as a genetically encoded secretory tracer. In particular, when expressed in liver hepatocytes *in vivo*, albumin-fused fluorescent tracers should be incorporated into the blood via large fenestrated hepatic capillaries.

Plasma is robustly and chronically visualized by *in vivo* hepatocyte transgene expression

To achieve *in vivo* expression of Alb-mNG in the liver, an AAV serotype 8 (AAV8) was utilized owing to its high affinity to hepatocytes.[18–21] The minimal transthyretin promoter P3 was used to achieve hepatocyte-specific expression (Fig 2a).[22,23] We confirmed strong hepatocytic expression of the AAV by systemic injection of AAV8-P3-eGFP (Fig 2d, i.v., 2 x 10^{11} vg, 3 weeks post-injection). Liver exhibited high eGFP expression in virtually all hepatocytes (Fig 2d) in agreement with previous reports.[24] We find that the fluorescence signal of AAV8-P3-Alb-mNG-infected liver was relatively mild, most likely due to the secretory nature of Alb-mNG (Fig 2d).

We next examined the presence of Alb-mNG in blood plasma. Blood samples were collected over an eight week period after AAV8 administration (Fig 2a,b). Examination of blood samples in glass micropipettes showed that the fluorescence signal can be detected as early as two days after injection and become brighter on the fifth day (Fig 2b). Longitudinal quantification of plasma fluorescence showed that the signal peaks at 3–4 weeks post-injection and the expression lasts over eight weeks (one-way ANOVA: significant effect of time, $p<0.05$; n=6 mice; Fig 2c). Plasma concentrations of mNG and albumin were further quantified during the eight-week timeframe (Fig 2e-f). Quantitative fluorescence measurements using known concentrations of mNG as reference shows a similar temporal profile of mNG plasma concentration to our glass-pipette assay, generally indicating ~1 µM plasma alb-mNG at two weeks or after post-injection (one-way ANOVA: no significant effect of time, $p>0.05$; n=3 mice; Fig 2e). Moreover, total plasma albumin concentration (endogenous and Alb-mNG) was stable (two-way ANOVA: no significant effect of time, treatment or interaction, $p>0.05$; n=3-4 mice; Fig 2f) and within the range of the published murine serum albumin concentration (Fig 2f, 20–30 mg/mL = 300–450 µM) suggesting normal albumin-oriented osmotic homeostasis.[14]

Alb-mNG does not lead to inflammation *in vivo* or abnormal spontaneous behavior

To examine possible immune responses due the recombinant protein expression, we measured plasma C-reactive protein (CRP) levels, a standard systemic marker for tissue inflammation that is produced in the liver.[25,26] As a result, plasma CRP levels in AAV-injected mice were comparable to those of saline-injected controls (during eight weeks post-AAV injection; t-test $p>0.05$; n(control)=6, n(Alb-mNG)=12 mice; Fig

2g). To further assess possible tissue inflammation, we visualized liver macrophages and brain microglia by IBA1 immunohistochemistry (Fig 2h). Accordingly, the morphology of liver macrophages and brain microglia did not reveal any signs of inflammation in AAV8-injected mice (Fig 2h). Moreover, neither body weight nor open-field ambulatory behavior were impacted by AAV8-P3-Alb-mNG or AAV8-P3-IgKL four weeks post-administration (Supp Fig 1).[27] Taken together, these experiments demonstrate the minimal footprint of our plasma labelling approach on host physiology and behavior.

Alb-mNG is superior to fluorescent-conjugated dextran for chronic study of circulation and vasculature

Having confirmed the plasma fluorescence by a single i.p. AAV injection, we imaged the cerebral vasculature of AAV-injected mice through a chronic cranial window (Fig 3a). Consistent with the plasma measurements, blood plasma was visualized by two-photon microscopy for at least eight weeks after AAV injection. To compare Alb-mNG fluorescence with acutely administrated fluorescent dyes, we administered Texas Red dextran (70k Da) to mice expressing Alb-mNG (Fig 3a&b). The labeled dextran showed a perfect match to the vascular pattern visualized by Alb-mNG ten minutes after administration. However, the signal intensity dropped substantially during the first hour of imaging. By contrast, Alb-mNG yielded a stable signal during the two-hour recording session (two-way ANOVA: probe x time interaction, $p<0.05$; *post hoc* tests: mNG-Alb vs Texas Red, $p<0.05$ at both 1h and 2h time points; n=3; Fig 3c). To further evaluate the utility of Alb-mNG for the longitudinal monitoring of vasculature, the cortical microvasculature was imaged at 3 and 7 weeks after AAV administration. While the vast majority of the microvasculature remained structurally similar across the imaging sessions, a few examples of vascular plasticity were noted (Fig. 3d&e). The robust visualization of blood plasma allows for the longitudinal study of microcirculation. To this end, we conducted high frame rate imaging (160-220 Hz) on selected areas containing a single capillary. We demonstrate that the expression of the albumin-fusion tracer reaches the levels required for this fast imaging regime several weeks post AAV injection. Indeed, captured capillary images show clear black and white stripes where the black areas indicate the presence of red blood cells (RBCs) three and seven weeks after AAV injection in the same animal (Fig 3f,h). Travel time between two points in a capillary was estimated by calculating the cross-correlogram of the time-signal intensity data (Fig 3g,i), hence the mean flow speed of 1.1 mm/s and 5.2 mm/s were computed for the two example captures.[7] These values were within the previously reported mean flow speed range.[7,28] To further evaluate the utility of liver-secreted plasma tracers, we imaged the microvasculature in the whisker-barrel cortex while stimulating whiskers. We demonstrate that functional hyperemia can be induced in the plasma-labeled mice by whisker stimulation, as previously shown (Fig. 3h).[29,30] Our method allows chronic assessment of functional hyperemia for more than seven weeks after AAV administration (two-way ANOVA: vessel type x time interaction, $p<0.05$; at both first and second whisker stimulation; n(arteries)=3, n(veins)=3 from 3 mice; Fig. 3i-j).

To address the importance of the molecular size of liver-secreted plasma fluorescent tracer, we also expressed IgKL-mNG in the liver using the same AAV8 approach (Supp Fig 2). Long-term visualization of blood plasma was also possible with this viral construct, however, plasma fluorescent intensity was an order of magnitude lower than that of Alb-mNG (Supp Fig 2 b&d) pointing toward the importance of the molecular size for vascular leakage. Quantification of total albumin revealed similar concentrations to controls and Alb-mNG (Supp Fig 2 c) with no signs of systemic inflammation (Supp Fig 2 e&f). Despite the decreased plasma fluorescence compared to Alb-mNG, imaging of cerebral vasculature was feasible (Supp Fig 2 g) including fast capillary imaging for RBC flow (Supp Fig 2 h).

To extend the toolbox of Alb-fused proteins as a chronic plasma tracers, we designed a new vector by substituting mNG with a bright red fluorescent protein mScarlet[31] (Alb-mScarlet). As with Alb-mNG

systemic administration of AAV8-P3-Alb- mScarlet (i.v., via the retro-orbital sinus) achieved robust long-term plasma visualization by two-photon microscopy. Furthermore, we have also successfully generated albumin-fused tracers with rosmarinus (cyan),[32] and mCarmine (deep red),[33] which are available via Addgene (see Methods) (Supp Fig 3).

Besides cerebral vasculature, long-term monitoring of vasculature in peripheral tissue is also possible. We demonstrate this by imaging vasculature in the ear. [34] Even at ten weeks after a single i.p. injection of Alb-mNG viral construct, signal is strong enough even for fast imaging of capillary RBC flow (Supp Fig 4).

Finally, we tested whether our fluorescent tracers are adequate for macroscopic study of cerebral vasculature. Major vessels on the brain surface can be readily imaged through a cranial window using a macroscope four weeks after AAV administration of both Alb-mScarlet and Alb-mNG (Fig. 4a).[12] Notably, the image contrast between vessels and parenchymal background is enhanced in Alb-mScarlet resulting in a significantly higher signal to noise ratio of vascular imaging (Signal/background ratio: Mann Whitney: $p<0.05$; Shannon's entropy: Mann Whitney: $p<0.05$; n(Alb-mNG)=10, n(Alb-mScarlet)=6 mice; Fig. 4b-c).

Discussion

Chronic monitoring of the vasculature is crucial for the study of developmental processes,[35,36] brain states,[37] aging[38] as well as disease progression,[39,40] recovery,[41] and evaluation of therapeutic effects. Currently, imaging of the vasculature requires repeated intravenous injection of dextran-conjugated fluorescent dyes. Here we present a novel genetic approach that enables robust labeling of plasma for more than three months. A single i.p. or i.v. injection of AAV induces hepatocyte expression of fluorescent protein-tagged albumin and achieves labelling of blood plasma. No additional manipulations are required, making this approach ideal for the study of both wild type and genetically modified mice. We present four implementations of this approach using the monomeric fluorescent proteins mNeonGreen (Alb-mNG), mScarlet (Alb-mScarlet), mCarmine (Alb- mCarmine) and Rosmarinus (Alb- Rosmarinus), and demonstrate that fluorescent protein-tagged albumin is superior to dextran-conjugated fluorescent dyes. A key strength is the minimally invasive and long-lasting nature of this approach. While our monitoring period was limited by our animal experimentation license, previous studies report sustained AAV-mediated gene expression for over nine months.[21] This suggests that the AAV-mediated plasma probes can be used to track the vasculature for a significant portion of the rodent lifespan.

A crucial advantage of the novel approach introduced in this study is the ease to collect more physiologically relevant data compared to acutely injected tracers such as fluorescent dextran. Our genetic approach diminishes the induced stress and complications from repeated i.v. injections especially when performed on awake mice. While we did not directly measure viscosity in blood samples, our quantification of recombinant and total albumin in the plasma suggests that viscosity change by the current protocol is unlikely since the total albumin level remains virtually unchanged for the observation period of several months (Fig 2f). Therefore, the expression of albumin fusion probes avoids the documented concern about blood viscosity increase by dextrans infusion.[8,9] Moreover, no signs of systemic or tissue inflammation were noted as assessed by histology and the CRP assay. In addition, unaltered open-field activity and body weight strongly supports the suitability of the plasma probe for chronic experiments. Of note, the recombinant albumin is derived from the murine albumin sequence with an intention to minimize immune reactivity in mice.

Undoubtedly, the most exciting application of genetically encoded plasma visualization is the longitudinal study of vascular circulation. Coupling with functional imaging of distinct cell types such as endothelial

cells, pericytes, or astrocytes, is expected to provide new insights into various processes pertinent to circulation including angiogenesis and vascular plasticity.[42–44] The technique accommodates experimental designs that span several months with lasting plasma signal intensity. The high signal-to-noise ratio and long-term expression achieved by the current method should enable daily assessment of changes of blood circulation and BBB permeability. For macroscopic imaging, Alb-mScarlet has a clear advantage compared to Alb-mNG due to the brightness of mScarlet, low intrinsic fluorescence of the brain in the red spectra, and the reduced tissue scattering of longer wave lengths.[31]

We find that i.p. injection yields reliable plasma probe expression, likely reflecting that the primary route of AAV particle absorption is through the mesenteric vessels, which drain into the portal vein of the liver.[45] If this is the case, i.p.-injected AAV particles reach hepatocytes before entering systemic circulation. While lower quantities of viral constructs are needed for retro-orbital injections (1/3 of i.p.), i.p. injection offers a few advantages including simpler procedure, shorter administration time, adaptability to awake animals, and higher reproducibility.[46] The low biosafety level of AAV usage makes it possible to use this method in all standard laboratories. Moreover, the prevalence of AAV technology has made this technique financially affordable.

Here, we present four implementations of liver-secreted fusion protein approach. The ever-growing toolbox of optical biosensors and optical manipulation tools combined with advances in miniaturized microscopy provide huge opportunities for the longitudinal study of circulation in a near-physiological manner. Coupled with rodent disease models, liver-secreted biosensors and other genetically encoded tools open the way for exploring causal relationships between circulation and disease pathophysiology.

Materials and Methods

Mice

C57BL/6JRj mice (Javier) of either sex in an age range of 1.5-6 months were used. Mice were housed in 12-h light/12-h dark cycle (lights on: 7am) with food and water *ad libitum*. The procedures involving animal care, surgery, *in vivo* imaging, and sample preparation were approved by the local research ethics committee (Department of Experimental Medicine, University of Copenhagen) and conducted in accordance with the Danish Animal Experiments Inspectorate.

DNA constructs

Mouse albumin (*Alb*) nucleotide sequence was obtained from the NIH nucleotide database (NCBI Reference Sequence: NM_009654.4). The IgK leader (*IgKL*) and mNeonGreen (mNG) nucleotide sequences were obtained from the Addgene web site (plasmids 177814 and 128144, respectively). mNG-Alb was constructed by concatenating the Alb and mNG sequences with the linker sequence SmaI-scFv-AgeI, where scFV represents the (Gly4Ser) x3 amino acid sequence coded by GGT GGA GGC GGT TCA GGC GGA GGT GGC TCT GGC GGT GGC GGA TCA. Likewise, Alb-mNG was constructed by concatenating the mNG and Alb sequences with the linker sequence SmaI-scFv-SalI. The construction for secretory mNG protein IgKL-mNG achieved by concatenation of a shortened IgKL signal peptide (MTDTLLLWVLLLWVPGSTGD) to mNG. mNG-Alb, Alb-mNG, and IgKL-mNG were artificially synthesized and cloned into a mammalian expression vector (Twist Bioscience, pTwist CMV Betaglobin WPRE Neo). For all fusion protein constructs, the first methionine codon was removed from the second protein sequence. The tertiary structure of Alb-mNG was predicted by the Phyre2 program using the intensive mode.[47]

pAAV-CBh-Alb-mNG and pAAV-CBh-IgKL-mNG were constructed by ligating the insert to the AAV backbone vector pAAV/CBh_*-WPRE-SV40pA (Viral Vector Core, Gunma University Initiative for

Advanced Research) via the AgeI and NotI sites. pAAV-P3-Alb-mNG and pAAV-P3-IgKL-mNG were made using pAAV-P3-EGFP as a template (p438, Viral Vector Facility VVF, Institute of Pharmacology and Toxicology, University of Zurich). pAAV-P3-Alb-mScarlet was made by replacing mNeonGreen with mScarlet (sequence from Addgene plasmid #174185 with a silent mutation to eliminate the NotI site within the mScarlet cDNA). The artificially synthesized DNA segment containing the partial sequence Alb-scFV and mScarlet was subcloned into pAAV-P3-Alb-mNeonGreen via NdeI and EcoRI. AAVs encoding Alb-mNG or IgKL-mNG were produced using the ultracentrifugation method as described previously.[48] The titers of purified AAVs were as follows: AAV8-P3-Alb-mNG (3.99×10^{13} vg/mL), AAV8-P3-IgKL-mNG (2.67×10^{13} vg/mL), AAV8-P3-Alb-mScarlet (1.65×10^{13} vg/mL). AAV8-P3-EGFP was obtained from VVF (v438, 4.5×10^{12} vg/mL). pAAV plasmids are made available via Addgene (pAAV-P3-Alb-mNG #183460; pAAV-P3-Alb-mScarlet #183461; pAAV-P3-Alb-rosmarinus #183462; pAAV-P3-Alb-mCarmine #183464; pAAV-P3-IgKL-mNG #183465; pAAV-CBh-Alb-mNG #183466; pAAV-CBh-IgKL-mNG #183467).

Cell culture

HEK293T cells (Dharmacon, HCL4517), cultured in DMEM supplemented with 10% FBS and 50 U/mL penicillin-streptomycin (Thermo Fisher Scientific, 41965039, 16141079 and 15140122), were transfected in a 24-well plate using Fugene HD (Promega, E2311) at 30% confluency. For each well, transfection reagent was mixed with 0.5 µg of plasmid DNA at a 3:1 ratio (µL/µg) in 25 µL Opti-MEM (Thermo Fisher Scientific, 31985070) and added dropwise after 15-minute incubation at room temperature. Each transfection was carried out in six replicates. Cells were imaged under the microscope (Nikon Eclipse Ti) at 24 h and 48 h after transfection. To evaluate secretion of expressed molecular tracers, the ratio of extracellular and cytosolic fluorescence intensity was calculated. To further quantitate the secretion of molecular tracers, 200 µL of culture medium was collected from each well and centrifuged for five minutes at 1200 rpm, 100 µL of the supernatant was subjected to fluorescent measurements in a black 96-well plate (Thermo Fisher Scientific, 437796) using a SpectraMax iD3 microplate reader (Molecular Devices, excitation/emission at 485/538 nm). The cell culture medium was collected 24 h and 48 h after transfection from separate sets of cells.

In vivo recombinant protein expression

Long-term *in vivo* transgenes expression in the liver was achieved by systemic administration of AAV, up to 6×10^{11} vg in 0.3–0.6 mL sterile phosphate buffered saline (PBS). Intraperitoneal injection (i.p.), or intraveneous injection (i.v.) via the tail vein or retroorbital sinus was performed. For tail vein i.v. injection, mice were briefly anesthetized with isoflurane (~1-2%) and mounted in a stereotactic frame. Retroorbital injections were performed according to the protocol by Yardeni et al.[49] after a brief anesthesia with isoflurane. Mice were recovered in the home cage thereafter. Other *in vivo* transfection methods such as hydrodynamic transfection using pCAG DNA plasmids nor liposome-based transfection using a commercial reagent did not result in sufficient or sustained expression for the detection of fluorescence in the plasma.

Biochemical analysis

Blood sampling and plasma extraction

To prevent clotting of the blood, heparin (500U, LEO) was injected i.p. to deeply anesthetized mice thirty minutes prior to perfusion-fixation. Total of 0.5–0.7 mL blood was collected from the heart and stored in 0.75 mL tubes containing 5 µL EDTA and 5 µL Halt protease and phosphatase inhibitor cocktail (100x, Thermo Scientific). The tubes were centrifuged for 10 minutes (2000 x G, 4 ºC), and the supernatant was collected as plasma. Plasma samples were stored in aliquots at -80 °C until further imaging and analysis.

Plasma albumin quantification

Total plasma albumin concentration was determined using a commercially available enzyme-linked immune sorbent assay (ELISA) kit (Abcam, ab108792). The ELISA was performed according to the manufacture's protocol and the results were measured using a SpectraMax iD3 microplate reader (OD 450 nm). Sample duplicates were measured in 1:2,000,000 dilution and concentrations were calculated with Microsoft Excel using a four-parameter logistic curve-fit as recommended by the manufacturer.

Plasma mNG quantification

The mNG protein was purified from an *E.coli* expression system (Gene Universal, USA) and was reconstituted at varying concentrations ranging from 6.25 to 200 nM in PBS for calibration of mNG concentration (standard curve, triplicates). Plasma samples of Alb-mNG expressing mice were diluted at 1:10 in PBS. The fluorescence of samples was measured in duplicates using a SpectraMax iD3 plate reader (excitation 485 nm, emission 535 nm). mNG concentrations in plasma samples were calculated by the standard curve (linear fit).

Estimation of relative Alb-mNG proportion

The relative proportion of Alb-mNG in plasma samples was calculated from the assay results of total albumin and mNG concentrations. The albumin concentration was converted to molar concentration using the albumin molecular weight of 65.9 kDa. Then we divided the molar values of mNG by the molar values of albumin to obtain the relative proportion of total mNG for each sample. The relative proportion was plotted as percentage of total albumin concentration.

Plasma C-reactive protein assessment

To examine possible systemic inflammation in response to viral expression of Alb-mNG, plasma C-reactive protein (CRP) was measured using an ELISA (Invitrogen, EM20RB). The ELISA was performed according to the manufactures protocol and the results were measured using a SpectraMax iD3 microplate reader (OD 450 nm). In brief, sample duplicates were measured in 1:2000 dilutions. CRP concentrations were calculated using a four-parameter logistic curve-fit as recommended.

Ex vivo macro fluorescence imaging

To examine the development of fluorescent tracer expression in the same animals over a time course of 8 weeks, blood was sampled from the tail in borosilicate glass capillaries (1B100F-4 or 1B150F-4, WPI) and examined by a macroscope (Leica M205 FA) equipped with a X-Cite 200Dc light source, digital camera (C11440 Orca-flash 4.0, Hamamatsu). Filter sets ET GFP LP (excitation 480/40, emission 510LP, 10447407, Leica) and ET mCherry (excitation 560/40, emission 630/75m, 10450195, Leica) were used to image green or red channel, respectively. Images were acquired using Leica Application Suite X software (version 2.0.0.14332.2)

Open field test

The open field area is a square area of 40 x 40 cm^2 enclosed in a wooden box covered with white foam polyvinyl chloride. The inner area of 24 x 24 cm^2 is considered as arena center. Mice were transferred to the room one day before the experiment and tested at the end of the light cycle (5–7 pm). Mouse movement was recorded with a video camera placed above the open field box. The test was initiated by placing a single mouse in the center of the box, thereafter the mouse explored the arena freely for 10 min. The box was cleaned with alcohol and water after each session.

Histology

Deeply anesthetized mice (ketamine/xylazine 100 mg/kg and 20 mg/kg, respectively) were transcardially perfused with physiological saline briefly followed by 4% paraformaldehyde (PFA) in 0.1 M phosphate buffer (PB, pH 7.4) using a peristaltic pump. Body organs including liver and brain were harvested and post-fixed in 4% PFA overnight before further storage in PBS. 50 µm sections were prepared using a vibratome (Leica VT1200 S) in PBS. Brain sections were incubated with rabbit anti-IBA1 (WAKO WDE1198, 1:1000) and chicken anti-GFAP (Fisher Scientific- Invitrogen, PA1-10004, 1:1000) for microglia and astrocyte immunohistochemistry. Liver sections were incubated with rat anti-CD45 (Bio-Rad, MCA1388, 1:500) and rabbit anti-IBA1 for hepatic macrophages. Anti-mNG (chromotek 32F6, 1:1000) was used for the detection of mNeonGreen expression.

Primary antibodies were detected using the following secondary antibodies: Alexa Fluor 568 goat anti-chicken (Thermo Fisher Scientific, A11041, 1:1000), Alexa Fluor 594 goat anti-rabbit (Thermo Fisher Scientific- Invitrogen, A11012, 1:1000), Alexa Fluor 568 goat anti-rat (Abcam AB1755710, 1:1000). Stained tissue slices were mounted with antifade mounting medium with DAPI (Vector laboratories, Vectashield, H-1200). Images were acquired using a standard fluorescence microscope (Nikon ECLIPSE Ni-E) and a digital camera (Mono-Camera Nikon DS-Fi3) controlled by an imaging software (NIS-Elements Imaging software AR 4.60.00. Confocal images were acquired by a Nikon Eclipse Ti2 microscope with a Plan Apo x60/1.40 numerical aperture (NA) oil objective controlled by an imaging software NIS-Elements AR 4.50.00.

In vivo fluorescence imaging.

Cranial window surgery

Mice were anesthetized by 3-4% isoflurane for induction and then mounted to the stereotaxic frame. Throughout the surgery, the anesthesia was maintained at 1–1.5% isoflurane and the body temperature were maintained at 37 °C with a heating pad. The skull was exposed after applying local analgesia (lidocaine, 0.2 mg/mL) by making an incision to the scalp, and a metal frame (head plate) was then attached to the skull using dental cement (Super Bond C&B, Sun Medical, Shiga, Japan). A 4-mm diameter craniotomy above the somatosensory cortex was made and the dura mater was surgically removed. 4mm diameter autoclaved cover slip was carefully mounted to cover the brain and then sealed by dental cement. Mice were recovered in their home cage and received 24 h systemic analgesia in form of carprofen (5 mg/kg).

Two-photon microscopy

Two-photon imaging were performed on anesthetized (70 mg/kg ketamine, 10 mg/kg xylazine) or awake mice. For awake mouse imaging, mice were acclimatized to head fixation at least a week before the imaging experiments (MAG-1 or MAG-2, Narishige). To mount a mouse for awake imaging, the mouse was briefly anesthetized by 2% isoflurane and head plate fixation was secured in the microscopy apparatus. Imaging session started twenty minutes after the mouse was mounted under the objective lens.

The two-photon microscope setup consisted of a B-Scope (Thorlabs) equipped with a resonant scanner, a Chameleon Vision 2 laser (Coherent), an objective lens (Apo LWD 25 ×/1.10w, Nikon), and the primary dichroic mirror ZT405/488/561/680-1100rpc (Chroma) as described before.[50] Emission light was separated by the secondary dichroic mirror (FF562-Di03, Semrock) with band-pass filters FF03-525/50 and FF01-607/70 (both Semrock). mNG and mScarlet were excited at 940 nm and 1000 nm, respectively. For simultaneous imaging of mNG and Texas Red, FF01-647/70 (Semrock) was used for the red channel to avoid bleedthrough and the excitation wavelength was set at 950 nm. Images were acquired using ThorImage Software Version 3.0. The laser power under the objective lens was measured by a power meter (Thorlabs) before imaging to ensure consistent excitation across chronic monitoring of plasma tracer.

Comparison of plasma Alb-mNG and Texas-Red dextran was made using mice under anesthesia. After baseline volumetric imaging, Texas-Red dextran (70k MW, D1830, Invitrogen) was administered i.v. (retroorbital, 15 mg/mL in saline, 50 µL). Linear scaling of laser power with imaging depth was applied (power under the objective lens: 10–35 mW for 0–500 µm). Successive imaging was made at 10, 60, and 120 min.

Functional hyperemia imaging was performed with awake mice. Imaging and sensory stimulation were synchronized via a pulse generator (Master-9, A.M.P.I) connected to the B-Scope hardware. Whisker-evoked functional hyperemia in the barrel cortex was induced by presenting air puffs (50 ms duration, 10 Hz, 5 s, 30 PSI) to the mouse's whisker pad 30 s after the start of imaging. The pre-stimulus period served as baseline for later analysis. Each imaging session lasted at least for 70 s.

Capillary flow was captured by restricting the imaging area to a single capillary with non-averaged bidirectional scanning, achieving frame rates of up to 220 Hz. The excitation power under the objective lens was kept under 20 mW.

Fluorescence imaging by macroscope

The same macroscope for glass capillary imaging was used for imaging of coverslipped cranial window (Leica M205 FA) of AAV-injected mice. Briefly, mice were head fixed to a MAG-1 or MAG-2 headplate fixture apparatus and placed under the macroscope. Filter sets ET GFP LP (excitation 480/40, emission 510LP, 10447407, Leica) and ET mCherry (excitation 560/40, emission 630/75m, 10450195, Leica) were used to image green or red channel, respectively.

Image data analysis

To calculate the relative intensity between intracellular and extracellular fluorescence (Fig. 1D), cellular areas was detected by an adaptive threshold approach using the *imbinarize()* function in Matlab (Mathworks, USA) on greyscale-converted cell culture images. The mean intensity was calculated for the cellular area and compared with the extracellular mean intensity. Identical excitation intensity and exposure time was used for all time-points analyzed.

Vascular fluorescence for Texas-Red dextran and Alb-mNG (Fig. 3B&C) was calculated by first detecting vascular areas using the Otsu thresholding method applied to the 3D image stack using the *graythresh()* Matlab function. Mean intensity was calculated for the detected vascular areas. To compare different time points, mean intensity signals were normalized to the time point at 10 min after Texas Red dextran injection for each channel.

Red blood cell velocity (Fig. 3F) was estimated by computing the unbiased cross-correlogram of the intensity signals from two distant locations on the same capillary.[51] The time-intensity vectors of the two chosen points were transformed to z values to compute the correlation coefficients.

Arterial diameter dynamics for functional hyperemia experiments (Fig. 4 B&C) were determined as follows. First, the intensity profile along a manually selected line that intersects the target vessels was computed using the *improfile()* function in Matlab. The edges of the vessels were estimated by detecting the sharp intensity signal decreases, and the vessel diameter is calculated as the distance between the two edges. Computed vascular diameter function was normalized to the mean diameter during a 2-s period before sensory stimulation.

Signal-to-noise ratio (Fig. 4 b) was calculated as the ratio of vasculature fluorescence minus the parenchymal fluorescence divided by the parenchymal fluorescence. Vasculature was identified as previously, and mean signal was calculated as well as for the extra-vascular parenchyma. For Shannon's

entropy calculation, the image matrices were first converted to probability matrices by dividing by their total single intensities and custom function *info_entropy()* was used (Vallabha Hampiholi; Entropy Calculator; MATLAB Central File Exchange).

Statistics

All measured values are indicated as mean ± sem. Comparisons of two sample group means were assessed by t-test. Multiple group comparisons were performed using one-way or two-way ANOVA unless otherwise noted. Graph Prism 9 was used for all statistical analyses.

References

1. Mescher AL. The Circulatory System. In: *Junqueira's Basic Histology: Text and Atlas, 15e*. New York, NY: McGraw-Hill Education; 2018.

2. Schmidt RF. *Human Physiology*. 2nd ed. (Schmidt RF, Thews G, eds.). New York, NY: Springer-Verlag Berlin Heidelberg; 1989.

3. Grutzendler J, Nedergaard M. Cellular Control of Brain Capillary Blood Flow: In Vivo Imaging Veritas. *Trends in Neurosciences*. 2019;42(8):528–536.

4. Takano T, Tian G-F, Peng W, Lou N, Libionka W, Han X, Nedergaard M. Astrocyte-mediated control of cerebral blood flow. *Nature Neuroscience*. 2006;9(2):260–267.

5. Wei HS, Kang H, Rasheed I-YD, Zhou S, Lou N, Gershteyn A, McConnell ED, Wang Y, Richardson KE, Palmer AF, Xu C, Wan J, Nedergaard M. Erythrocytes Are Oxygen-Sensing Regulators of the Cerebral Microcirculation. *Neuron*. 2016;91(4):851–862.

6. Hudetz AG. Blood flow in the cerebral capillary network: a review emphasizing observations with intravital microscopy. *Microcirculation (New York, N.Y. : 1994)*. 1997;4(2):233–252.

7. Chaigneau E, Oheim M, Audinat E, Charpak S. Two-photon imaging of capillary blood flow in olfactory bulb glomeruli. *Proceedings of the National Academy of Sciences*. 2003;100(22):13081–13086.

8. Goldenberg M, Crane RD, Popper H. Effect of intravenous administration of dextran, a macromolecular carbohydrate, in animals. *American journal of clinical pathology*. 1947;17(12):939–948.

9. Grönwall A, Ingelman B. Dextran as a Substitute for Plasma. *Nature*. 1945;155(3924):45.

10. Swank RL, Escobar A. Effects of Dextran Injections on Blood Viscosity in Dogs. *Journal of Applied Physiology*. 1957;10(1):45–50.

11. Dormandy JA. Influence of blood viscosity on blood flow and the effect of low molecular weight dextran. *British medical journal*. 1971;4(5789):716–719.

12. Ahn SJ, Ruiz-Uribe NE, Li B, Porter J, Sakadzic S, Schaffer CB. Label-free assessment of hemodynamics in individual cortical brain vessels using third harmonic generation microscopy. *Biomedical optics express*. 2020;11(5):2665–2678.

13. Putnam FW. Progress in Plasma Proteins. In: *The Plasma Proteins: Structure, Function, and Genetic Control: Volume IV*. 2nd ed. Academic Press Inc.; 1984:1–44.

14. Zaias J, Mineau M, Cray C, Yoon D, Altman NH. Reference values for serum proteins of common laboratory rodent strains. *Journal of the American Association for Laboratory Animal Science : JAALAS*. 2009;48(4):387–90.

15. Schulze RJ, Schott MB, Casey CA, Tuma PL, McNiven MA. The cell biology of the hepatocyte: A membrane trafficking machine. *Journal of Cell Biology*. 2019;218(7):2096–2112.

16. Shaner NC, Lambert GG, Chammas A, Ni Y, Cranfill PJ, Baird MA, Sell BR, Allen JR, Day RN, Israelsson M, Davidson MW, Wang J. A bright monomeric green fluorescent protein derived from Branchiostoma lanceolatum. *Nature Methods*. 2013;10(5):407–409.

17. Schreiber G, Urban J. The synthesis and secretion of albumin. In: *Reviews of Physiology, Biochemistry and Pharmacology*. Berlin, Heidelberg: Springer Berlin Heidelberg; 1978:27–95.

18. Aronson SJ, Bakker RS, Shi X, Duijst S, ten Bloemendaal L, de Waart DR, Verheij J, Ronzitti G, Oude Elferink RP, Beuers U, Paulusma CC, Bosma PJ. Liver-directed gene therapy results in long-term correction of progressive familial intrahepatic cholestasis type 3 in mice. *Journal of Hepatology*. 2019;71(1):153–162.

19. Cunningham SC, Dane AP, Spinoulas A, Alexander IE. Gene Delivery to the Juvenile Mouse Liver Using AAV2/8 Vectors. *Molecular therapy : the journal of the American Society of Gene Therapy*. 2008;16(6):1081–1088.

20. Sands MS. AAV-mediated liver-directed gene therapy. *Methods in molecular biology (Clifton, N.J.)*. 2011;807:141–157.

21. Zincarelli C, Soltys S, Rengo G, Rabinowitz JE. Analysis of AAV serotypes 1-9 mediated gene expression and tropism in mice after systemic injection. *Molecular therapy : the journal of the American Society of Gene Therapy*. 2008;16(6):1073–1080.

22. Nair N, Rincon MY, Evens H, Sarcar S, Dastidar S, Samara-Kuko E, Ghandeharian O, Man Viecelli H, Thöny B, de Bleser P, VandenDriessche T, Chuah MK. Computationally designed liver-specific transcriptional modules and hyperactive factor IX improve hepatic gene therapy. *Blood*. 2014;123(20):3195–3199.

23. Viecelli HM, Harbottle RP, Wong SP, Schlegel A, Chuah MK, VandenDriessche T, Harding CO, Thöny B. Treatment of phenylketonuria using minicircle-based naked-DNA gene transfer to murine liver. *Hepatology (Baltimore, Md.)*. 2014;60(3):1035–1043.

24. Malato Y, Naqvi S, Schürmann N, Ng R, Wang B, Zape J, Kay MA, Grimm D, Willenbring H. Fate tracing of mature hepatocytes in mouse liver homeostasis and regeneration. *The Journal of clinical investigation*. 2011;121(12):4850–4860.

25. Liang C, Li J, Lu C, Xie D, Liu J, Zhong C, Wu X, Dai R, Zhang H, Guan D, Guo B, He B, Li F, He X, Zhang W, et al. HIF1α inhibition facilitates Leflunomide-AHR-CRP signaling to attenuate bone erosion in CRP-aberrant rheumatoid arthritis. *Nature Communications*. 2019;10(1):4579.

26. Pepys MB, Hirschfield GM. C-reactive protein: a critical update. *The Journal of Clinical Investigation*. 2003;111(12):1805–1812.

27. Burkholder T, Foltz C, Karlsson E, Linton CG, Smith JM. Health Evaluation of Experimental Laboratory Mice. *Current protocols in mouse biology*. 2012;2:145–165.

508 28. Unekawa M, Tomita M, Tomita Y, Toriumi H, Miyaki K, Suzuki N. RBC velocities in single
509 capillaries of mouse and rat brains are the same, despite 10-fold difference in body size. *Brain Research*.
510 2010;1320:69–73.

511 29. Rungta RL, Zuend M, Aydin A-K, Martineau É, Boido D, Weber B, Charpak S. Diversity of
512 neurovascular coupling dynamics along vascular arbors in layer II/III somatosensory cortex.
513 *Communications Biology*. 2021;4(1):855.

514 30. Takata N, Nagai T, Ozawa K, Oe Y, Mikoshiba K, Hirase H. Cerebral Blood Flow Modulation by
515 Basal Forebrain or Whisker Stimulation Can Occur Independently of Large Cytosolic Ca2+ Signaling in
516 Astrocytes. *PLOS ONE*. 2013;8(6):e66525.

517 31. Bindels DS, Haarbosch L, van Weeren L, Postma M, Wiese KE, Mastop M, Aumonier S, Gotthard
518 G, Royant A, Hink MA, Gadella TWJ. mScarlet: a bright monomeric red fluorescent protein for cellular
519 imaging. *Nature Methods*. 2017;14(1):53–56.

520 32. Molina RS, Tran TM, Campbell RE, Lambert GG, Salih A, Shaner NC, Hughes TE, Drobizhev M.
521 Blue-Shifted Green Fluorescent Protein Homologues Are Brighter than Enhanced Green Fluorescent
522 Protein under Two-Photon Excitation. *The Journal of Physical Chemistry Letters*. 2017;8(12):2548–2554.

523 33. Fabritius A, Ng D, Kist AM, Erdogan M, Portugues R, Griesbeck O. Imaging-Based Screening
524 Platform Assists Protein Engineering. *Cell Chemical Biology*. 2018;25(12):1554-1561.e8.

525 34. Honkura N, Richards M, Laviña B, Sáinz-Jaspeado M, Betsholtz C, Claesson-Welsh L. Intravital
526 imaging-based analysis tools for vessel identification and assessment of concurrent dynamic vascular
527 events. *Nature Communications*. 2018;9(1):2746.

528 35. Coelho-Santos V, Berthiaume A-A, Ornelas S, Stuhlmann H, Shih AY. Imaging the construction
529 of capillary networks in the neonatal mouse brain. *Proceedings of the National Academy of Sciences*.
530 2021;118(26):e2100866118.

531 36. Harb R, Whiteus C, Freitas C, Grutzendler J. *In Vivo* Imaging of Cerebral Microvascular Plasticity
532 from Birth to Death. *Journal of Cerebral Blood Flow & Metabolism*. 2013;33(1):146–156.

533 37. Turner KL, Gheres KW, Proctor EA, Drew PJ. Neurovascular coupling and bilateral connectivity
534 during NREM and REM sleep. *eLife*. 2020;9.

535 38. Ungvari Z, Tarantini S, Donato AJ, Galvan V, Csiszar A. Mechanisms of Vascular Aging.
536 *Circulation Research*. 2018;123(7):849–867.

537 39. Montagne A, Nikolakopoulou AM, Huuskonen MT, Sagare AP, Lawson EJ, Lazic D, Rege S v,
538 Grond A, Zuniga E, Barnes SR, Prince J, Sagare M, Hsu C-J, LaDu MJ, Jacobs RE, et al. APOE4 accelerates
539 advanced-stage vascular and neurodegenerative disorder in old Alzheimer's mice via cyclophilin A
540 independently of amyloid-β. *Nature Aging*. 2021;1(6):506–520.

541 40. Hill RA, Tong L, Yuan P, Murikinati S, Gupta S, Grutzendler J. Regional Blood Flow in the Normal
542 and Ischemic Brain Is Controlled by Arteriolar Smooth Muscle Cell Contractility and Not by Capillary
543 Pericytes. *Neuron*. 2015;87(1):95–110.

544 41. Williamson MR, Franzen RL, Fuertes CJA, Dunn AK, Drew MR, Jones TA. A Window of
545 Vascular Plasticity Coupled to Behavioral Recovery after Stroke. *The Journal of Neuroscience*.
546 2020;40(40):7651 LP – 7667.

547 42. Nikolakopoulou AM, Montagne A, Kisler K, Dai Z, Wang Y, Huuskonen MT, Sagare AP, Lazic
548 D, Sweeney MD, Kong P, Wang M, Owens NC, Lawson EJ, Xie X, Zhao Z, et al. Pericyte loss leads to
549 circulatory failure and pleiotrophin depletion causing neuron loss. *Nature Neuroscience*. 2019;22(7):1089–
550 1098.

551 43. Payne S, de Val S, Neal A. Endothelial-Specific Cre Mouse Models. *Arteriosclerosis, Thrombosis,*
552 *and Vascular Biology*. 2018;38(11):2550–2561.

553 44. Iadecola C, Nedergaard M. Glial regulation of the cerebral microvasculature. *Nature Neuroscience*.
554 2007;10(11):1369–1376.

555 45. Lukas G, Brindle SD, Greengard P. The route of absorption of intraperitoneally administered
556 compounds. *Journal of Pharmacology and Experimental Therapeutics*. 1971;178(3):562 LP – 566.

557 46. Turner P v, Brabb T, Pekow C, Vasbinder MA. Administration of substances to laboratory animals:
558 routes of administration and factors to consider. *Journal of the American Association for Laboratory Animal*
559 *Science : JAALAS*. 2011;50(5):600–613.

560 47. Kelley LA, Mezulis S, Yates CM, Wass MN, Sternberg MJE. The Phyre2 web portal for protein
561 modeling, prediction and analysis. *Nature Protocols*. 2015;10(6):845–858.

562 48. Konno A, Hirai H. Efficient whole brain transduction by systemic infusion of minimally
563 purified AAV-PHP.eB. *Journal of neuroscience methods*. 2020;346:108914.

564 49. Yardeni T, Eckhaus M, Morris HD, Huizing M, Hoogstraten-Miller S. Retro-orbital injections in
565 mice. *Lab Animal*. 2011;40(5):155–160.

566 50. Oe Y, Wang X, Patriarchi T, Konno A, Ozawa K, Yahagi K, Hirai H, Tsuboi T, Kitaguchi T, Tian
567 L, McHugh TJ, Hirase H. Distinct temporal integration of noradrenaline signaling by astrocytic second
568 messengers during vigilance. *Nature Communications*. 2020;11(1):471.

569 51. Chaigneau E, Oheim M, Audinat E, Charpak S. Two-photon imaging of capillary blood flow in
570 olfactory bulb glomeruli. *Proceedings of the National Academy of Sciences*. 2003;100(22):13081–13086.

571

572

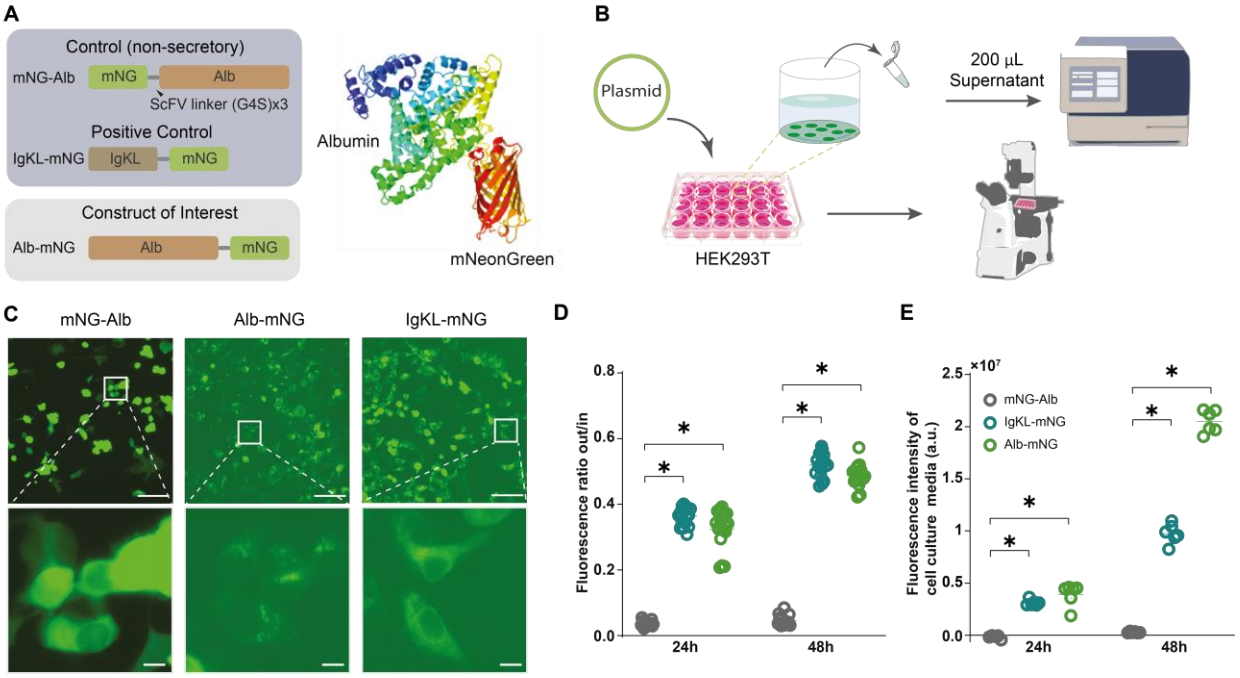

Figure 1. Construction and validation of secretory fluorescent protein-tagged albumin A) Schematic construct design of mNG-Alb (non-secretory negative control), IgkL-mNG (secretory positive control), and Alb-mNG. A 3D protein structure prediction for Alb-mNG is displayed on the right. B) Schematic illustration for cell culture testing of the plasmid constructs. C) Microscopic images of transfected HEK293T cells at 48 h for mNG-Alb, Alb-mNG, and IgKL-mNG. Scale bars 100 µm The lower row is the magnification of the corresponding white squares in the upper row. Scale bars 10 µm. D) Fluorescence signal ratio of external vs cytosolic signal of microscopic images taken at 24 h and 48 h N =18. E) Fluorescence intensity of cell culture medium from 24 h and 48 h post-transfection measured via a microplate reader. N =6. All graphs show means ± SEM; * $p < 0.05$.

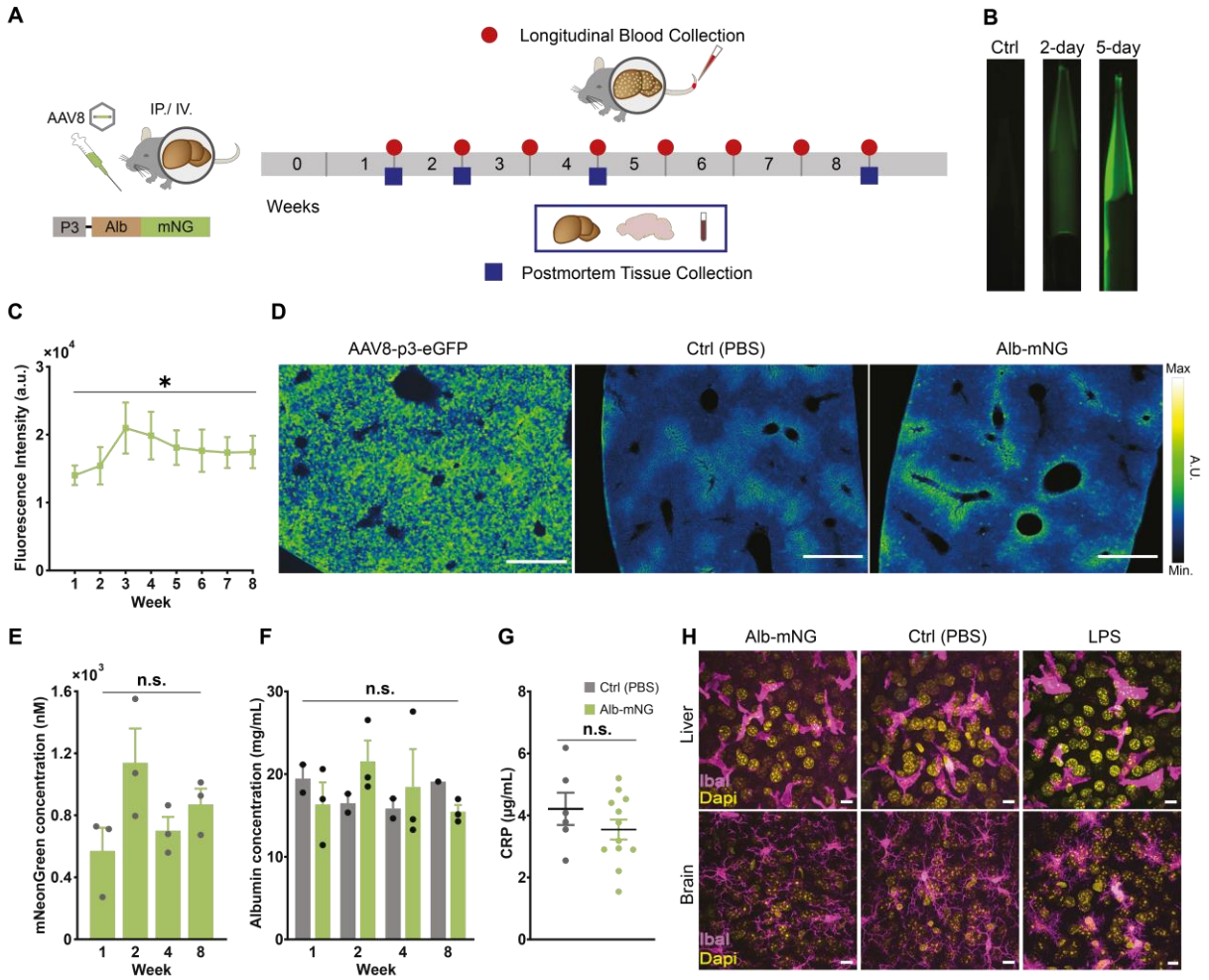

Figure 2. Robust and chronic visualization of blood plasma by *in vivo* transgene expression of Alb-mNG in hepatocytes. A) Schematic of approach for the *in vivo* experiments. AAV8-P3-Alb-mNG is administrated to mice via i.p. or i.v.injection (left). Alb-mNG expression was monitored by collecting blood sample from the tail. Brain and liver tissues and blood were collected for morphological and biochemical examination (right side). B) Example of the fluorescence signals in blood samples collected on day 2 and 5 from an Alb-mNG-injected mouse. C) Plasma Alb-mNG fluorescence intensity over a time course of 8 weeks (N = 6 mice). D) Mouse liver images after 3 weeks of AAV8-P3-eGFP (positive control), PBS (negative control), and AAV8-P3-Alb-mNG injection. Scale bar 500 μm. E) mNG concentration in plasma samples (N =3 mice each group). F) Plasma albumin concentration using albumin ELISA in PBS-injected (gray) and Alb-mNG injected (green) mice (N =3 mice each group). G) Plasma CRP levels for control or Alb-mNG injected mice during the 8 weeks of post-injection period (N =6–12). H) Example images of liver (top panel) and brain slices (lower panel) of control (PBS) or Alb-mNG mice immunostained for macrophages (liver) or microglia (brain) by IBA1 (purple) and DAPI (yellow). Brain sections of LPS-injected mice displayed reactive microglia morphology while resting microglia are observed in the Alb-mNG mouse. Scale bars 10 μm. All graphs show means ± SEM; * $p < 0.05$.

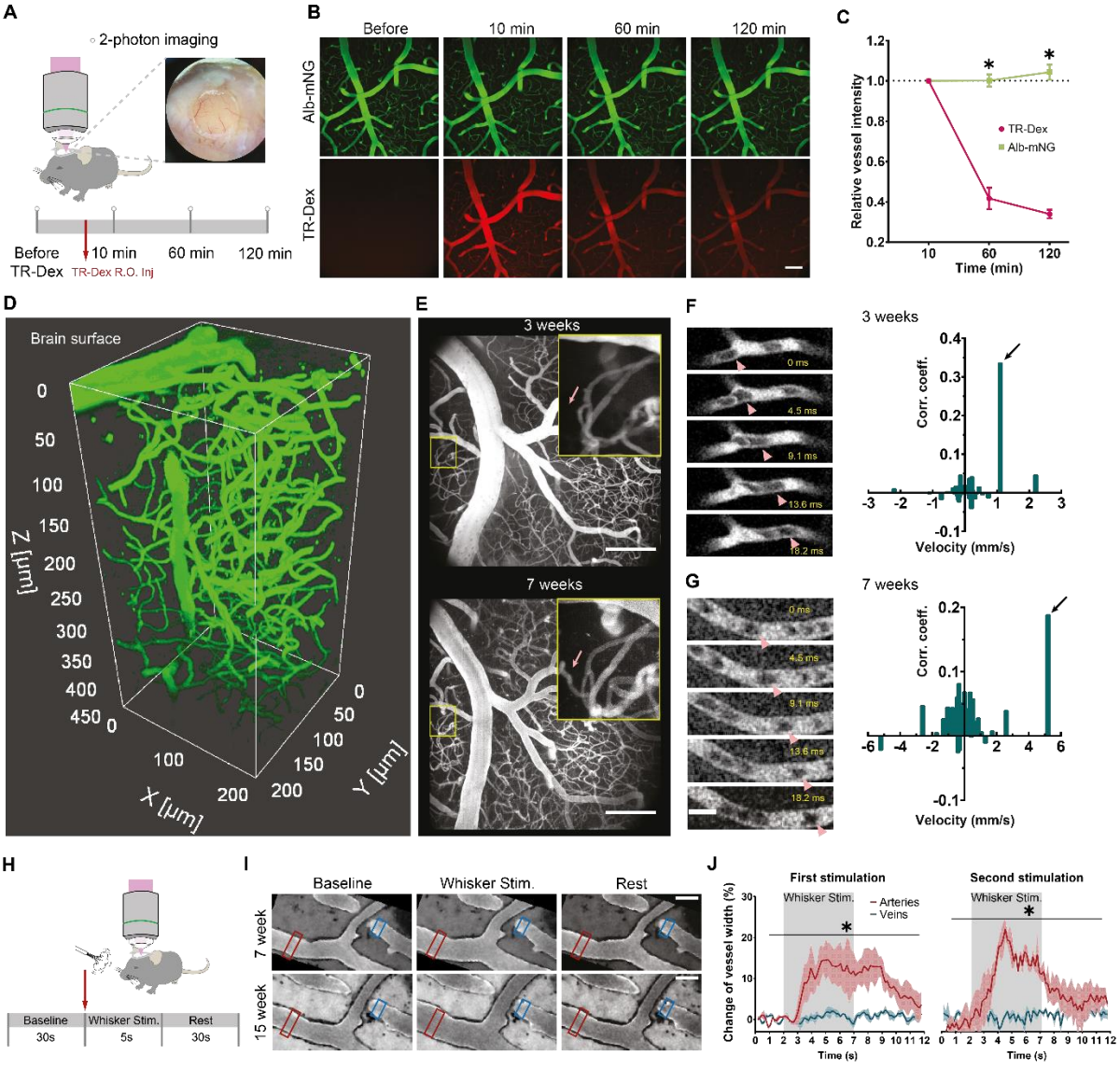

Figure 3. Genetic expression of Alb-mNG is advantageous to fluorescent dextran in long-lasting imaging sessions. A) Experimental approach to compare the genetically expressed Alb-mNG with i.v. injected Texas-Red dextran (70 kDa). Alb-mNG expressing mice (7–8 weeks) were imaged under ketamine-xylazine anesthesia before and 10, 60 and 120 min after Texas-Red dextran injection. B) Example images at various time points during an imaging session. Alb-mNG signal is present throughout the total imaging session with little attenuation. Texas-Red dextran signals diminishes within an hour. Scale bar 100 µm. C) Quantification of signal intensity for Alb-mNG and Texas-Red dextran for the time course of 120 min (N =3). D) Volumetric imaging of brain vasculature covering 450 µm below the pial surface of Alb-mNG-expressing mouse (post-injection 10 weeks). E) 2-photon images obtained from the same mouse at 3 and 7 weeks of Alb-mNG expression. The zoomed in area (yellow square) depicts neovascularization at 7 weeks (red arrow). Scale bar 100 µm. F-G) 2-photon imaging of a capillary at 3 and 7 weeks of Alb-mNG expression at frame rate of 116–220Hz enables quantification of blood flow velocity by computing the crosscorrelogram (right). see histogram to the right side. Pink triangles indicate the flow of an example red blood cell. Scale bar 10 µm. H) Experimental setup for functional hyperemia induced by whisker-puff. Two whisker stimulations, took place in each recording session. I) Example 2-photon images of the same mouse

at 7 weeks and 15 weeks expression of Alb-mNG show dilation of artery (marked in red square) compared to vein (marked in blue square) after air puff whisker stimulation. Scale bar 50 µm. C) Quantification of percentage change of vessel width (N =3) for artery and vein after two whisker stimulations (50ms pulse for 5s each; inter-stimulation period = 30min). All graphs show means ± SEM; * $p < 0.05$.

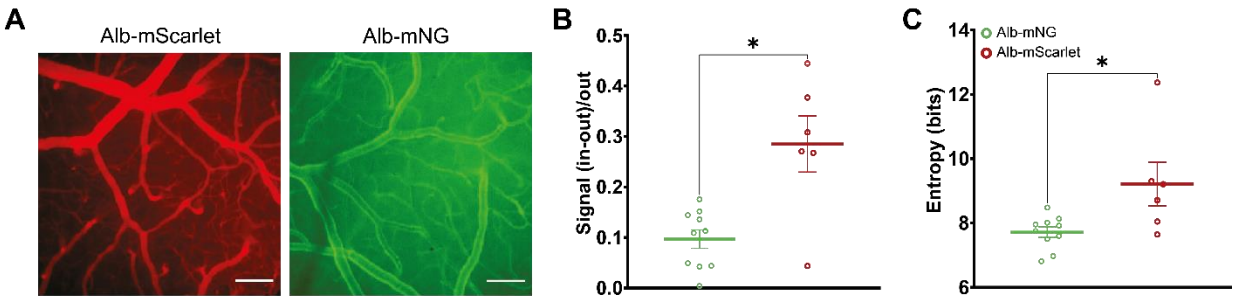

Figure 4. Comparison between Alb-mNG and Alb-mScarlet macroscopic fluorescent imaging. A) Representative examples of macroscopic imaging with the two fluorescent plasma probes four weeks after AAV administration. B) Signal-to-noise ratio quantification. C) Shannon's entropy of macroscopic images. Scale bars 50 µm. All graphs show means ± SEM; * $p < 0.05$.

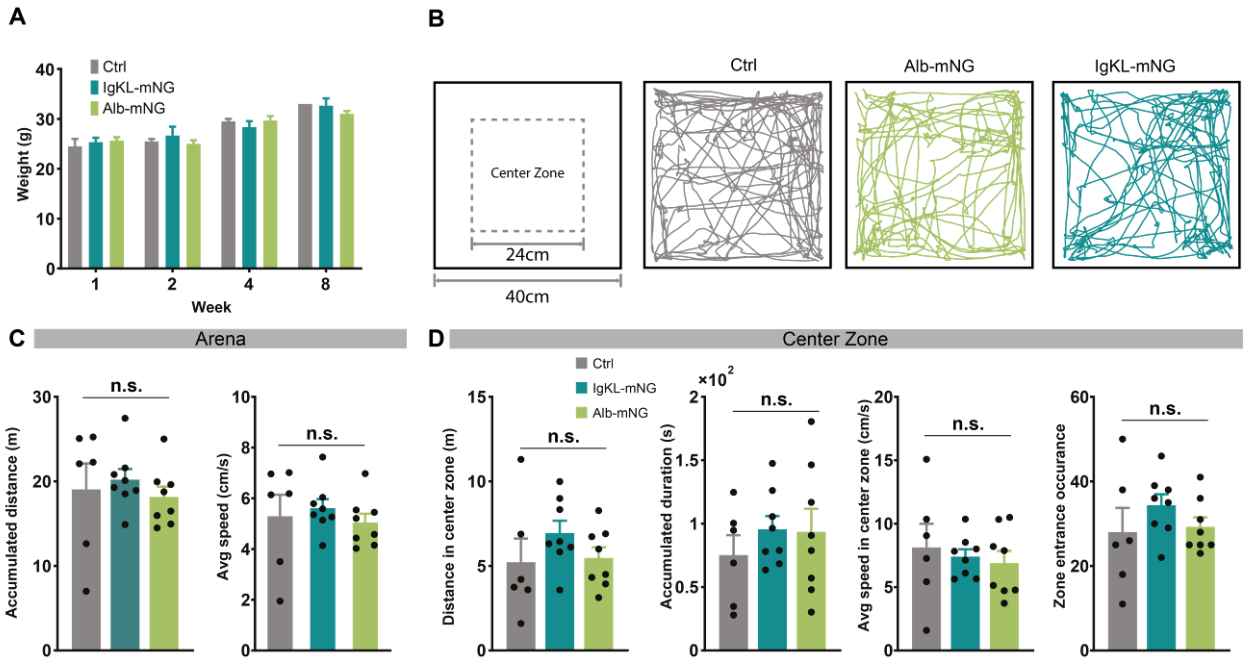

633

634 **Supplementary Figure 1. Plasma tracer expression does not display obvious phenotypes in body**
635 **weight or open field behavior** A) Body weight of control (age matched sham) and AAV-P3-IgKL-mNG-
636 injected and AAV8-P3-Alb-mNG-injected mice during 1 to 8 weeks post-injection. AAV-injected mice
637 show no differences in body weight compared to control; two-way ANOVA: significant main effect of
638 time, no significant main effect of group or group x time interaction; n=3 mice per group B) Schematic of
639 the arena used for open field test and example traces of mouse trajectory for 10 min. C) Total distance
640 traveled (left) and mean speed of movement (right) during the 10 min of open field behavior; one-way
641 ANOVA: no significant main effect of group; n=6-8 mice per group. D) Metrics on center zone behavior.
642 Distance moved, total time, speed of movement, and frequency of visiting the center zone did not show
643 significant differences among control and AAV injected mice; one-way ANOVA: no significant main effect
644 of group for all metrics; n=6-8 mice per group. All graphs show means ± SEM; * $p < 0.05$.

645

646

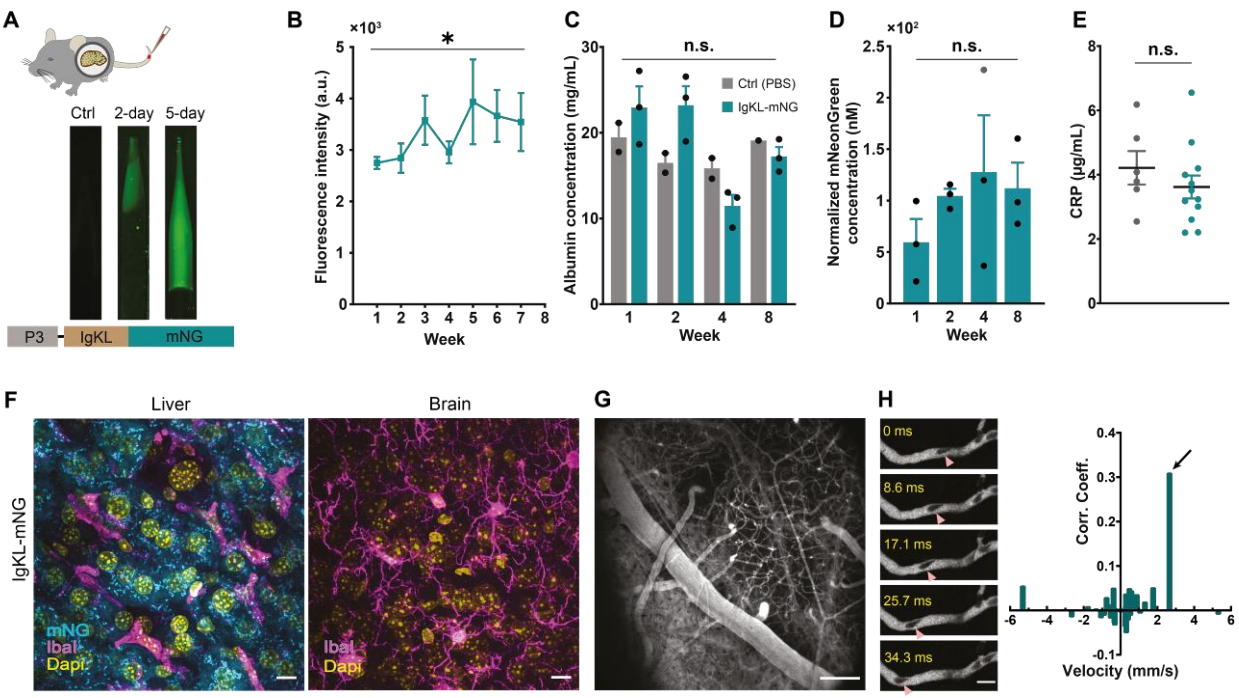

Supplementary Figure 2. Liver-targeted expression IgKL-mNG (secretory mNG). A) A secretory form of mNeonGreen, IgKL-mNG, is expressed in the liver by systemic injection of AAV8-P3-IgKL-mNG in mice. Fluorescence signals were detected in the blood samples two days after AAV injection. (B) Chronic monitoring of plasma fluorescence. Note that the plasma intensity is an order of magnitude lower than Alb-mNG (Fig. 2) one-way ANOVA: significant effect of time, $p<0.05$; n=6 mice. (C) Plasma albumin concentration and plasma mNG concentration (D) over eight weeks; Albumin concentration: two-way ANOVA: no significant effect of time, group or interaction, $p<0.05$; mNG concentration: one-way ANOVA: no significant effect of time, $p<0.05$; n=3 mice. E) CRP levels during the 8 weeks of post-AAV injection period is indistinguishable from sham-injected control. (t-test $p>0.05$; n(control)=6, n(IgKL-mNG)=12. F) Liver and brain images 3 weeks after AAV injection. Immunofluorescence: mNG (blue), IBA1 (mangenta), DAPI (yellow). Scale bar 10 µm. G) 2-photon imaging through a cranial window visualizes cerebral blood vasculature despite the relatively low fluorescence signal intensity. (H). Capillary blood flow is also quantifiable using IgKL-mNG as a plasma tracer (RBC speed = 2.65 mm/s). All graphs show means ± SEM; * $p < 0.05$.

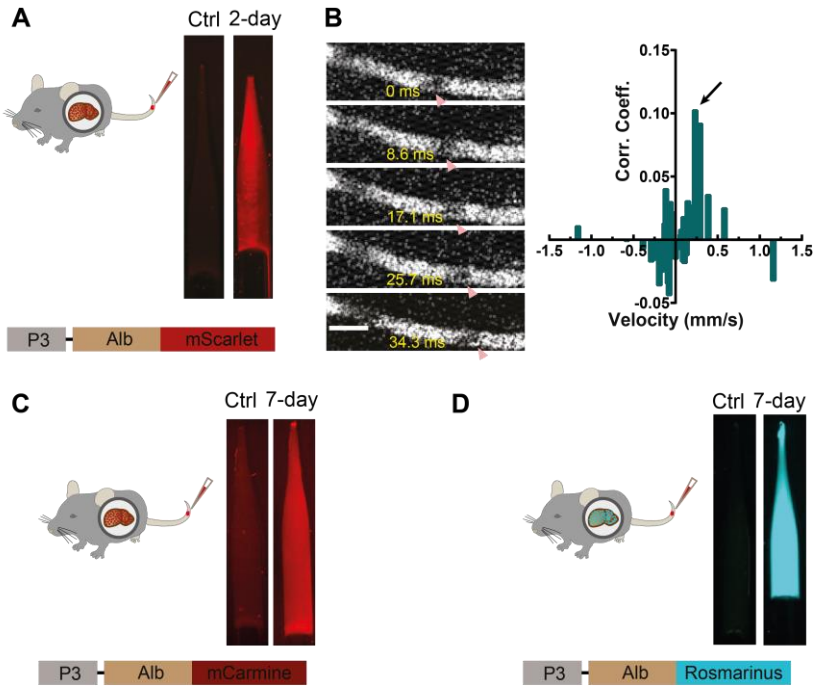

Supplementary Figure 3. Expanding the spectrum of liver-secreted plasma fluorescent probes. A) Systemic injection of AAV8-P3-Alb-mScarlet results in labeling of blood plasma with red fluorescence, thereby representing a plasma tracer that is spectrally distinct from Alb-mNG. B) Capillary flow dynamics is reliably visualized by 2-photon microscopy (RBC speed = 0.25 mm/s). Alb-based plasma tracer spectrum is further extended by the addition of and Alb-mCarmine (deep red fluorescence) (C), and Alb-Rosmarinus (cyan fluorescence) (D).

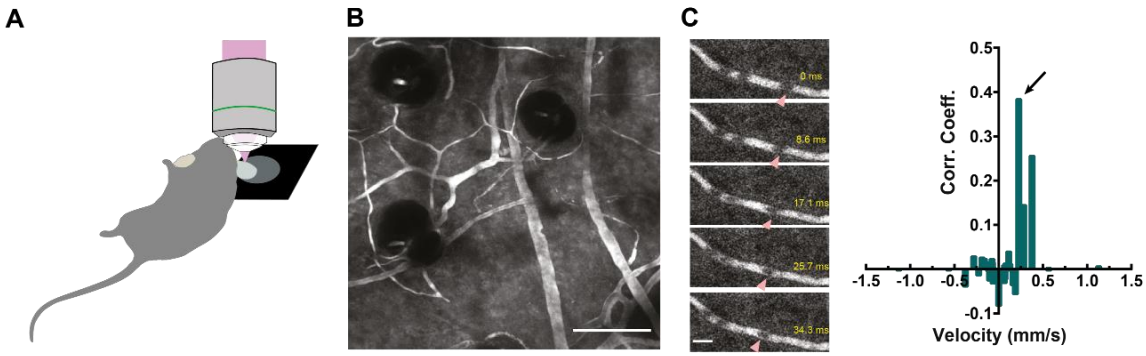

Supplementary Figure 4. Alb-mNG is suitable for studying vasculature in peripheral tissues. A) Schematic of 2-photon imaging of the ear skin capillary network in an Alb-mNG expressing mouse under ketamine-xylazine anesthesia. B) Example image of ear vasculature. The black holes are the cavity space for hair follicle. C) Measurement of blood flow in peripheral ear capillary via 2-photon imaging, (RBC speed = 0.23 mm/s)